Verticillin A Causes Apoptosis and Reduces Tumor Burden in High-Grade Serous Ovarian Cancer by Inducing DNA Damage

Amrita Salvi[1], Chiraz Soumia M. Amrine[2], Julia R. Austin[1], KiAundra Kilpatrick[1], Angela Russo[1], Daniel Lantvit[1], Esther Calderon-Gierszal[1], Zachary Mattes[3], Cedric J. Pearce[4], Mark W. Grinstaff[3], Aaron H. Colby[3], Nicholas H. Oberlies[2], and Joanna E. Burdette[1]

ABSTRACT

High-grade serous ovarian cancer (HGSOC) is the most lethal gynecological malignancy in women worldwide and the fifth most common cause of cancer-related deaths among U.S. women. New therapies are needed to treat HGSOC, particularly because most patients develop resistance to current first-line therapies. Many natural product and fungal metabolites exhibit anticancer activity and represent an untapped reservoir of potential new agents with unique mechanism(s) of action. Verticillin A, an epipolythiodioxopiperazine alkaloid, is one such compound, and our recent advances in fermentation and isolation are now enabling evaluation of its anticancer activity. Verticillin A demonstrated cytotoxicity in HGSOC cell lines in a dose-dependent manner with a low nmol/L IC_{50}. Furthermore, treatment with verticillin A induced DNA damage and caused apoptosis in HGSOC cell lines OVCAR4 and OVCAR8. RNA-Seq analysis of verticillin A–treated OVCAR8 cells revealed an enrichment of transcripts in the apoptosis signaling and the oxidative stress response pathways. Mass spectrometry histone profiling confirmed reports that verticillin A caused epigenetic modifications with global changes in histone methylation and acetylation marks. To facilitate *in vivo* delivery of verticillin A and to monitor its ability to reduce HGSOC tumor burden, verticillin A was encapsulated into an expansile nanoparticle (verticillin A-eNP) delivery system. In an *in vivo* human ovarian cancer xenograft model, verticillin A-eNPs decreased tumor growth and exhibited reduced liver toxicity compared with verticillin A administered alone. This study confirmed that verticillin A has therapeutic potential for treatment of HGSOC and that encapsulation into expansile nanoparticles reduced liver toxicity.

Introduction

Ovarian cancer is the fifth leading cause of death among women and is the most lethal tumor type of the female reproductive tract (1). In 2019, an estimated 22,530 women in United States will be diagnosed with ovarian cancer and about 13,980 women will succumb to the disease (2). The most common and deadly histologic subtype of ovarian cancer is high-grade serous ovarian cancer (HGSOC). Current treatment for HGSOC entails cytoreductive surgery and chemotherapy. However, most patients develop chemoresistance and ultimately die from recurrent disease. Chemoresistance is multi-faceted and likely arises both from mechanisms of resistance to the current therapy, paclitaxel and carboplatin, or through immune cell evasion (3–6).

One avenue to identify new therapies that may avert the chemoresistance problem is through the investigation of natural product drug leads with both unique chemical structures and modes of action, such as the verticillins (7). The verticillins are epipolythiodioxopiperazine alkaloids, and largely exist as dimers containing both diketopiperazine moieties and disulfide bridges. This group of secondary metabolites is usually isolated from terrestrial and marine filamentous fungi, such as *Verticillium sp.*, *Penicillium sp.*, and *Gliocladium sp*. that belong to Sordariomycetes and Eurotiomycetes (8, 9). Verticillin A was the first discovered analogue in 1970, and to date, 27 verticillin analogues are described in the literature (8–10).

Enabled by recent advances in fungi fermentation and isolation, the role of verticillin A as an anticancer agent is actively being investigated (8, 11). Verticillin A induces cytotoxicity in human breast carcinoma, large-cell lung carcinoma, astrocytoma, colorectal adenocarcinoma, and melanoma cell lines (8). Mechanistically, verticillin A selectively inhibits histone methyltransferases (HMTases) such as SUV39H1, SUV39H2, G9a, HTM, MLL1, and GLP (12, 13). In colon carcinoma, verticillin A inhibited H3K9 methylation on the *FAS* promoter, restored Fas expression, and caused cell death by apoptosis (12). Furthermore, mice treated with a combination of verticillin A and 5-fluorouracil displayed significantly smaller tumors and sensitized metastatic colon carcinoma cells to 5-fluorouracil (12). In addition, verticillin A suppressed metastatic colon cancer cell immune evasion and chemoresistance (12). In pancreatic cancer cells, verticillin A inhibited MLL1, a HMTase responsible for H3K4 methylation, leading to decreases in H3K4me3 levels and PD-L1 expression. Lower PD-L1 expression led to reduced binding to PD-1 and activation of an immune response along with an enhanced chemotherapeutic response (13). In a recent study with pancreatic ductal adenocarcinoma cells, verticillin A differentially altered H3K9me3 and H3K4me3 levels leading to expression of proapoptotic genes and inhibition of antiapoptotic genes (14).

Because verticillin A acts through a variety of HMTases resulting in epigenome changes by histone marks, the genomic landscape of

[1]Department of Pharmaceutical Sciences, College of Pharmacy, University of Illinois at Chicago, Chicago, Illinois. [2]Department of Chemistry and Biochemistry, University of North Carolina at Greensboro, Greensboro, North Carolina. [3]Departments of Chemistry, Biomedical Engineering, and Medicine, Boston University, Boston, Massachusetts. [4]Mycosynthetix Inc., Hillsborough, North Carolina.

Note: Supplementary data for this article are available at Molecular Cancer Therapeutics Online (http://mct.aacrjournals.org/).

Corresponding Author: Joanna E. Burdette, University of Illinois at Chicago, 900 S. Ashland Rm 3202, Chicago, IL 60607. Phone: 312-996-6153; Fax: 312-996-7107; E-mail: joannab@uic.edu

Mol Cancer Ther 2020;19:89–100

doi: 10.1158/1535-7163.MCT-19-0205

different tumor types that arise from different tissues will dictate gene expression; thus, defining the anticancer action. Therefore, to determine whether ovarian cancer might respond to this class of compounds, this study focused on the mode of action of verticillin A in HGSOC cells. Verticillin A induced cell death in HGSOC cells and, when encapsulated into a nanoparticle, it reduced toxicity and tumor burden *in vivo*. Specifically, verticillin A altered histones, significantly changed gene expression, and induced DNA damage via oxidative stress. DNA damage leading to γH2.AX foci occurred rapidly and cotreatment with n-acetyl-cysteine blocked apoptosis caused by verticillin A. Animals treated with verticillin A–loaded expansile nanoparticles (verticillin A-eNPs) reduced tumor burden *in vivo* and showed no morphologic signs of liver toxicity compared with free verticillin A. Together, these findings validate verticillin A as a potential anticancer compound with a novel mechanism of action in HGSOC and highlight verticillin A-eNPs as a promising drug delivery strategy.

Materials and Methods

Verticillin A purification and synthesis of expansile nanoparticles

Verticillin A (Supplementary Fig. S3A) was isolated and characterized from *Clonostachys rogersoniana* (strain MSX59553) as detailed previously following a recently published fermentation optimization strategy (8, 11). The purity of the isolated verticillin A was assessed via UPLC and ^{1}H-NMR (Supplementary Fig. S3B and S3C). The synthesis of verticillin A-eNPs and eNPs was performed using a miniemulsion polymerization method (Supplementary Fig. S2A) as described previously (15–17). Scanned electron microscope images were taken (Supplementary Fig. S2B), and a calibration curve of verticillin A was built to calculate the encapsulation efficiency, which was found to be 76.9% (Supplementary Fig. S2C). These data demonstrate the presence of 0.9 mg of verticillin A/mL of the expansile nanoparticles solution. Nanoparticles were stored at 4°C until the time of dosage.

Compounds/reagents

Verticillin A, UNC0638 (Sigma #U4885), and taxol/paclitaxel (Sigma #T7402) were resuspended in DMSO. N-Acetyl-L-cysteine (Sigma #A9165) was freshly prepared using sterile deionized water. Hydrogen peroxide (H_2O_2) (Thermo Fisher Scientific #H325) was freshly diluted with the media before addition to the cells. Final vehicle concentration < 0.1% (v/v).

Cell culture

OVCAR8 and OVCAR8-RFP [OVCAR8 cells expressing red fluorescent protein (RFP)] were a gift from Sharon Stack at the University of Notre Dame (Notre Dame, Indiana) and immortalized human ovarian surface epithelial cells (IOSE80) were a gift from Nelly Auersperg at the University of British Columbia (Vancouver, British Columbia, Canada). Normal human fallopian tube cells FT33 were a gift from Ronny Drapkin at the University of Pennsylvania (Philadelphia, PA). OVSAHO cells (Japanese Cell Bank) were grown in RPMI1640 supplemented with 10% FBS and penicillin/streptomycin (final concentration: 100 I.U./mL and 100 μg/mL, respectively). OVCAR4 cells (NCI) were grown in RPMI1640 supplemented with L-glutamine (2 mmol/L), 10% FBS, and penicillin/streptomycin. OVCAR8, OVCAR8-RFP, HEPG2, and U87 cells were grown in DMEM with 10% FBS and penicillin/streptomycin. IOSE80 cells were grown in v/v 50% Medium 199 and v/v 50% MCBD with 15% FBS, penicillin/streptomycin, L-glutamine (2 mmol/L), and 11 ng/mL epithelial growth factor. FT33 cells were grown in DMEM-Ham's F12 supplemented with penicillin/streptomycin and 2% Ultroser-G. All cultured cells were *Mycoplasma* free and validated by short tandem repeat analysis in 2017. Cells were passaged a maximum of 20 times and maintained in a humidified incubator at 37°C in a 5% CO_2 environment.

Cell viability assay

A total of 3,000 cells were seeded in triplicates in a clear flat–bottomed 96-well plate and allowed to attach overnight. Compounds were suspended in DMSO and added to the cells. Cells were incubated for 24, 48, and 72 hours in the cell culture incubator and fixed with 20% Trichloroacetic acid. Cell viability was determined using 0.04% Sulforhodamine B via colorimetric detection at 505 nm (18). Normalization was performed using vehicle control (DMSO) and dose–response curves were generated using GraphPad Prism software.

Spheroid assay

OVCAR8 cells were trypsinized and 5,000 cells were resuspended in 80 μL of media per well in 96-well round bottom Ultra Low Attachment Plate (Corning 07-201-680). After 4 days, the spheroids were treated with 20 μL of compound for 72 hours and the plates were incubated at 37°C for 7 days. The plate was equilibrated to room temperature for 30 minutes and 100 μL of CellTiter-Glo 3D Reagent (Promega) was added. The plate was incubated on a shaker for 30 minutes to obtain complete lysis and luminescence was recorded using Synergy Mx Plate Reader (BioTek).

Histone profiling

Cells were seeded in 10-cm dishes and treated with verticillin A and vehicle control (DMSO) for 24 hours. Cells were pelleted, washed with PBS, and epiproteomic histone modification profiling was performed at Northwestern Proteomics Core Facility at Northwestern University (Evanston, IL) as described previously (19). Relative abundance (%) of histone marks was calculated on the basis of peptide peak areas extracted from the raw LC/MS data obtained.

RNA-sequencing

RNA was isolated from verticillin A and vehicle (DMSO)-treated cells using Qiagen RNAeasy Mini kit (#74104) as per the manufacturer's protocol. RNA libraries (3 technical replicates/treatment) were created. RNA quality determination, mRNA enrichment, library construction, sequencing, and transcriptome statistical analysis were performed at the Genomics Core Facility at Northwestern University.

cDNA synthesis and qRT-PCR analysis

Total RNA (1 μg) was converted to cDNA using iScript cDNA Synthesis Kit (Bio-Rad). qRT-PCR measurements were performed using the CFX connect Real-Time PCR Detection System (Bio-Rad) and SYBR Green (Roche) according to the manufacturer's protocol. Samples were normalized to the housekeeping gene, *GAPDH*. qRT-PCR primer sequences are mentioned in **Table 1**.

Alkaline comet assay

Agarose coated slides were prepared using 1% agarose (Thermo Fisher Scientific # BP160) and allowed to dry. Cells were trypsinized, washed in PBS, and resuspended in 0.5% low melting agarose (Sigma # A9414). A total of 300 μL of cell suspension was added to the coated slide to form a thin uniform layer and allowed to gel at 4°C for 30 minutes. Cells were lysed by incubating the slides for 3 hours with

Table 1. qRT-PCR primers.

Target gene	Forward primer sequence (5′-3′)	Reverse primer sequence (5′-3′)
TXN	TGAAGCAGATCGAGAGCAAGAC	TTCATTAATGGRGGCRRCAAGC
DUSP6	CCTGAGGCCATTTCTTTCATAGA	GTCACAGTGACTGAGCGGCTAAT
NFKB2	GAACAGCCTTGCATCTAGCC	TCCCAGTCGCTATCAGAGG
RELB	TCCCAACCAGGATGTCTAGC	AGCCATGTCCCTTTTCCTCT
TXNRD1	GAAGATCTTCCCAAGTCCTATGAC	ATTTGTTGCCTTAATCCTGTGAGG

chilled lysis buffer (2.5 mol/L NaCl, 0.1 mol/L EDTA, 10 mmol/L Tris pH 10, 1% N-lauroylsarcosine, 0.5% Triton X-100). Cells were subjected to alkaline electrophoresis (25 V, 300mA, 40 minutes) using electrophoresis buffer (300 mmol/L NaOH, 1 mmol/L EDTA, pH 13) at 4°C. Slides were coated with neutralization buffer (0.5 mol/L Tris pH 7.5) and stained with 2 μg/mL ethidium bromide, washed, and covered with a coverslip before visualization. Images were acquired using 20× objective on a Nikon Eclipse E600 microscope using DS-Ri1 digital camera and NIS Elements Software (Nikon Instruments). Comet tail moments were analyzed by TriTek CometScore software.

Reactive oxygen species detection assay

Cells plated on glass coverslips were treated with verticillin A, H_2O_2, and vehicle control (DMSO). CellROX Green Reagent (Invitrogen) was added (final concentration 5 μmol/L) and incubated for 30 minutes at 37°C. Cells were washed with PBS and fixed with 4% paraformaldehyde. Images were acquired using 40× objective on a Nikon Eclipse E600 microscope using a DS-Ri1 digital camera and NIS Elements Software (Nikon Instruments).

2D foci assay

A total of 200 cells were seeded in a 60-mm plate and allowed to attach overnight. Cells were treated with verticillin A and vehicle control (DMSO) for 8 hours. Following 15 days incubation, cells were fixed using 4% paraformaldehyde and stained with 0.05% crystal violet. Plates were washed using distilled water to minimize background. Images were acquired using FlourChem E System (ProteinSimple). Colonies were counted using ImageJ (imagej.nih.gov).

Immunoblot analysis

Cell lysates were prepared using RIPA lysis buffer (50 mmol/L Tris pH 7.6, 150 mmol/L NaCl, 1% Triton X-100, 0.1% SDS) supplemented with protease (Roche Applied Science #4693159001) and phosphatase (Sigma-Aldrich #P0044) inhibitors. Concentration of protein in lysates was determined by Bradford Assay (Bio-Rad #5000205) and proteins were resolved on SDS-PAGE gel. Proteins were transferred to nitrocellulose membrane and blocked in 5% nonfat milk. Primary antibody (**Table 2**) was incubated with the membrane overnight at 4°C. Membrane was washed and incubated in secondary antibody (**Table 3**) conjugated with horseradish peroxidase (HRP). The membrane was washed, and protein bands were detected with SuperSignal West Femto Substrate (Thermo Fisher Scientific #34095) and imaged on a FluorChem E System (ProteinSimple).

Table 2. Primary antibodies.

Antibody	Source	Dilution for WB	Dilution for immunofluorescence/IHC
Anti-rabbit PARP	CST #9542	1:1,000	—
Anti-rabbit cPARP	CST #9541	—	1:100 (IHC)
Anti-rabbit γH2A.X	CST #9718	1:500	1:100 (IHC, IF)
Anti-rabbit Bax	CST #5023	1:500	—
Anti-rabbit actin	Sigma #A2066	1:5,000	—

Abbreviations: CST, Cell Signaling Technology; IF, immunofluorescence; WB, Western blotting.

Immunofluorescence analysis of γH2.AX foci

Cells grown on glass coverslips were fixed using 4% paraformaldehyde, permeabilized with 0.2% TritonX-100, and blocked with 1% BSA in PBS. Cells were then incubated with γH2.AX primary antibody (diluted in blocking solution) for 1 hour at room temperature. The cells were washed with washing buffer (PBS with 0.05% TritonX-100) and then incubated with fluorescent secondary antibody (diluted in blocking solution) for 1 hour at room temperature. Cells were washed thrice with washing buffer. Nuclei were stained with DAPI (0.1 μg/mL; Thermo Fisher Scientific # EN62248) for 10 minutes at room temperature. Cells were washed using washing buffer and coverslips were mounted on glass slides using mounting media (Vector Laboratories #H-1000). Images were acquired using 40× objective on a Nikon Eclipse E600 microscope using DS-Ri1 digital camera and NIS Elements Software (Nikon Instruments).

Annexin V/propidium iodide staining

Cells were seeded in a 60-mm plate and allowed to attach overnight. Cells were treated with verticillin A, taxol, and vehicle control (DMSO) for 24 hours. Media were collected and cells were trypsinized and subjected to Annexin V-FITC/Propidium Iodide Apoptosis Assay (Nexcelom Biosciences) according to the manufacturer's instructions. K2 Cellometer was used to detect fluorescence using FCS express software. Gating channels were applied as per the manufacturer's protocol.

Mitochondrial toxicity assay

HEPG2 (hepatocellular carcinoma) and U87 (glioblastoma) cell lines were used to determine whether verticillin A caused mitochondrial toxicity, as mitochondrial toxicity is prone to occur in the brain and liver tissue. Mitochondrial toxicity was evaluated using a Promega

Table 3. Secondary antibodies.

Antibody	Source	Dilution for WB	Dilution for immunofluorescence
Anti-rabbit IgG-HRP	CST #7074	1:10,000	—
Anti-rabbit Alexa Fluor 488	Invitrogen #A-11034	—	1:1,000

Abbreviations: CST, Cell Signaling Technology; WB, Western blotting.

Mitochondrial ToxGlo kit according to the manufacturer's protocol. Briefly, 10,000 cells/well were seeded in 96-well plates in either glucose (25 mmol/L) or galactose (10 mmol/L) supplemented media and allowed to adhere for 8 hours. Cells were incubated with dilutions of oligomycin A (positive control) and verticillin A for 90 minutes prior to assay. Cells were incubated for 30 minutes with a cell impermeable, fluorogenic substrate, and fluorescence (Ex/Em 485/525 nm) was measured. Lysis buffer was added, and net ATP levels were determined by luminescence measurement.

Animals and xenograft experiments

All animals were treated in accordance with NIH Guidelines for the Care and Use of Laboratory Animals and the established Institutional Animal Use and Care protocol at the University of Illinois (Chicago, IL). Xenograft studies utilized NCr *nu*/*nu* athymic female mice 6–8 weeks in age (Taconic). Mice were housed in a temperature- and light-controlled environment (12 hours light and 12 hours dark) and provided food and water *ad libitum*. For xenograft experiments, OVCAR8-RFP cells (5×10^6) were injected intraperitoneally per mouse and tumor growth was monitored using Xenogen IVIS Spectrum *In Vivo* Imaging System (PerkinElmer) as described previously (20). Once all the mice formed tumors (~4 weeks), the mice were separated into two treatment groups and dosed once every 2 days with 0.5 mg/kg of verticillin A encapsulated nanoparticles (eNP-VA) and empty nanoparticles (eNP) for a total of 12 days. Mice were IVIS imaged twice weekly (535 nm excitation, and 620 nm emission, exposure time: 2 seconds, F stop: 2). Living Image 4.0 software was used to quantify the average abdominal radiant efficiency and normalization was performed using day 0 radiant efficiency. At week 7, all animals were sacrificed and tumors were collected for histologic analysis.

Tumor IHC

Tumors were fixed with 4% paraformaldehyde followed by dehydration and paraffin embedding. Paraffin blocks were sectioned using standard histologic procedures. Hematoxylin and eosin staining (H & E) and IHC were performed as described previously (21). Sections were incubated with primary antibody (**Table 2**) followed by incubation with biotin-conjugated secondary antibody (**Table 3**). Sections were developed using 3,3-diaminobenzidine to enable chromogenic detection. Tissues with primary antibody treatment were used as a negative control. Images were acquired on a Nikon Eclipse E600 microscope using a DS-Ri1 digital camera and NIS Elements Software (Nikon Instruments).

Statistical analysis

Data presented are mean ± SEM and represent at least three independent biological replicates. Statistical analysis was carried out using GraphPad Prism software. Statistical significance was determined by Student unpaired *t* test, one-way ANOVA, or two-way ANOVA with Dunnett multiple comparisons or Tukey *post hoc* test as mentioned in figure legends. $P < 0.05$ was considered statistically significant (*, $P < 0.05$; **, $P < 0.01$; ***, $P < 0.001$; ****, $P < 0.0001$).

Results

Verticillin A induces cytotoxicity in HGSOC cell lines *in vitro*

Verticillin A has been shown to inhibit the growth of colon cancer, pancreatic cancer, leiomyosarcoma, and malignant peripheral nerve sheath tumor cells (12–14, 22). To determine whether verticillin A inhibited growth of ovarian cancer cells, three validated models of HGSOC, OVSAHO, OVCAR4, and OVCAR8 were used. Taxol was used as positive control. Verticillin A was found to inhibit the growth of all three cell lines with IC_{50} values of 60 nmol/L, 47 nmol/L, and 45 nmol/L in OVSAHO, OVCAR4, and OVCAR8, respectively (**Fig. 1A**). To determine whether the growth inhibition was due to cytotoxic effects exerted by verticillin A, a 2D foci assay was performed. Cells were treated with verticillin A for 8 hours and foci were allowed to form for 2 weeks. As shown in **Fig. 1B**, treatment with verticillin A completely abrogated foci formation in OVCAR4 and OVCAR8 cells compared with vehicle control, suggesting a cytotoxic effect and not a cytostatic effect. Furthermore, to determine whether verticillin A affected cell viability of tumor spheroids, OVCAR8 spheroids were generated and treated with vehicle (DMSO), verticillin A, taxol, and cisplatin. A spheroid viability assay was performed, and it was found that verticillin A treatment caused disintegration of OVCAR8 spheroids. As shown in **Fig. 1C**, verticillin A treatment reduced spheroid viability with an IC_{50} value of 234 nmol/L.

RNA-sequencing analysis shows upregulation of apoptosis and oxidative stress in verticillin A–treated OVCAR8 cells

To further investigate whether verticillin A induced cytotoxicity through apoptotic cell death, annexin V-FITC (AV) and propidium iodide (PI) staining was performed. As shown in **Fig. 2A**, verticillin A treatment significantly increased the rate of early apoptosis (AV+, PI−) in both OVCAR4 and OVCAR8 cells relative to vehicle control. Consistent to the annexin V/propidium iodide staining, treatment with verticillin A markedly increased level of cleaved PARP (cPARP), a marker for apoptosis (**Fig. 2B**). Together, these results indicated that verticillin A inhibited growth of HGSOC cells by causing early apoptosis.

Studies in pancreatic and colon cancer cells demonstrated that verticillin A alters histone modifications likely through inhibiting HMTases and reducing H3K9me3 levels to increase expression of Bax, a proapoptotic protein (14, 23). Importantly, due to inhibition of HMTases and the genomic landscape of tumors, other targets such as Fas and PD-L1 were investigated in verticillin A–treated HGSOC cell lines and were not significantly different. Because Bax was consistently changed in all cell lines studied in the literature, we investigated its expression and found that verticillin A treatment increased Bax expression (Supplementary Fig. S1A). To confirm whether histones were modified, a global histone modification profiling was performed using mass spectrometry. OVCAR8 cells were treated with verticillin A and vehicle control (DMSO) for 24 hours and the relative abundance of 20 different posttranslational histone modifications were quantified by LC/MS analysis. Verticillin A induced 13 histone modifications including a reduction in H3K9me2, which was consistent with findings reported in colon cancer cells (Supplementary Fig. S1B). To further define the significance of histone modifications on global transcription, an RNA-sequencing analysis was performed with verticillin A–treated OVCAR8 cells. A total of 9,196 genes were found to be significantly altered by verticillin A treatment demonstrating that this molecule causes major genome-wide alterations in gene expression. Compared with vehicle control, a significant upregulation of apoptosis and oxidative stress pathway genes were observed in verticillin A–treated cells (**Fig. 2C**). qRT-PCR analysis was performed to validate the top hits from apoptosis and oxidative stress pathway (Supplementary Fig. S1C). Gene set enrichment analysis (GSEA) of the transcriptome identified the reactive oxygen species (ROS) pathway to be significantly upregulated in verticillin A–treated cells (**Fig. 2D** and **E**).

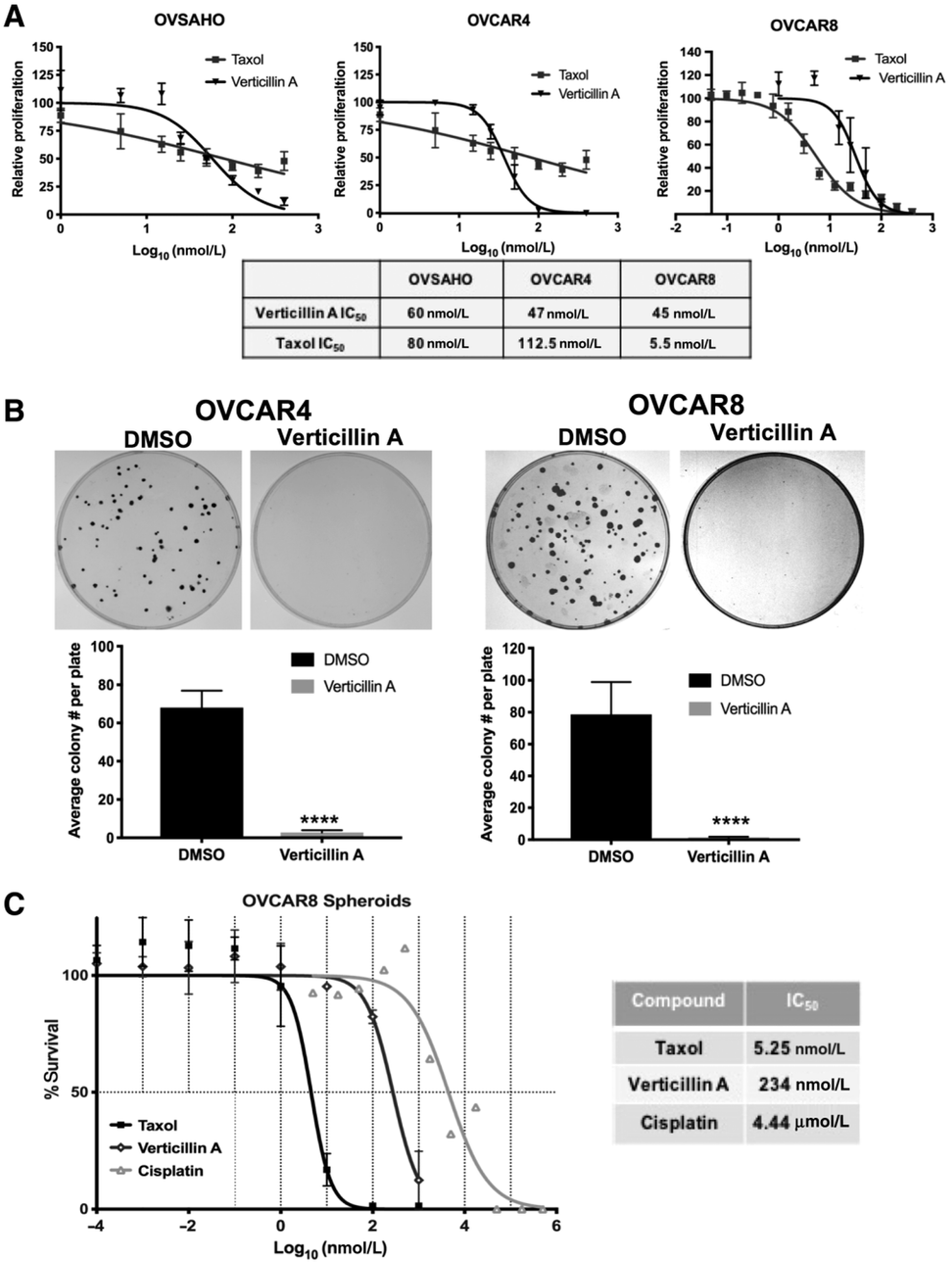

	OVSAHO	OVCAR4	OVCAR8
Verticillin A IC_{50}	60 nmol/L	47 nmol/L	45 nmol/L
Taxol IC_{50}	80 nmol/L	112.5 nmol/L	5.5 nmol/L

Compound	IC_{50}
Taxol	5.25 nmol/L
Verticillin A	234 nmol/L
Cisplatin	4.44 μmol/L

Figure 1.

Verticillin A induces apoptosis in HGSOC cell lines *in vitro*. **A,** OVSAHO, OVCAR4, and OVCAR8 cells were treated with vehicle (DMSO), verticillin A (50 nmol/L), and chemotherapeutic control taxol (10 nmol/L) for 72 hours. Dose–response curves were generated and normalized to vehicle control. IC_{50} values are denoted in the table. **B,** OVCAR4 and OVCAR8 cells were treated with vehicle and verticillin A (50 nmol/L) for 8 hours. Following drug incubation, media was changed and cells were incubated for 2 weeks to form colonies. Representative images of 2D foci assay performed in OVCAR4 and OVCAR8 cells are shown. Each experiment was performed in three biological replicates, and data represent mean ± SEM. Significance tested by Student *t* test in comparison to vehicle control. **C,** OVCAR8 spheroids were treated with vehicle, verticillin A, taxol, and cisplatin for 72 hours. Spheroid viability was determined using CellTiter-Glo Cell Viability assay. IC_{50} values are denoted in the table. Data represent mean ± SEM from two biological replicates.

Verticillin A causes oxidative stress and DNA damage in HGSOC cells without inducing mitochondrial toxicity

Verticillin A caused apoptosis in OVCAR4 and OVCAR8 cells and RNA-sequencing identified apoptosis and oxidative stress pathways to be significantly upregulated in OVCAR8 cells (**Fig. 2C** and **D**). Because alterations in ROS had not been previously reported, the effect of verticillin A on ROS generation was examined by using the CellROX reagent, a cell-permeable fluorogenic probe. Upon oxidation, the

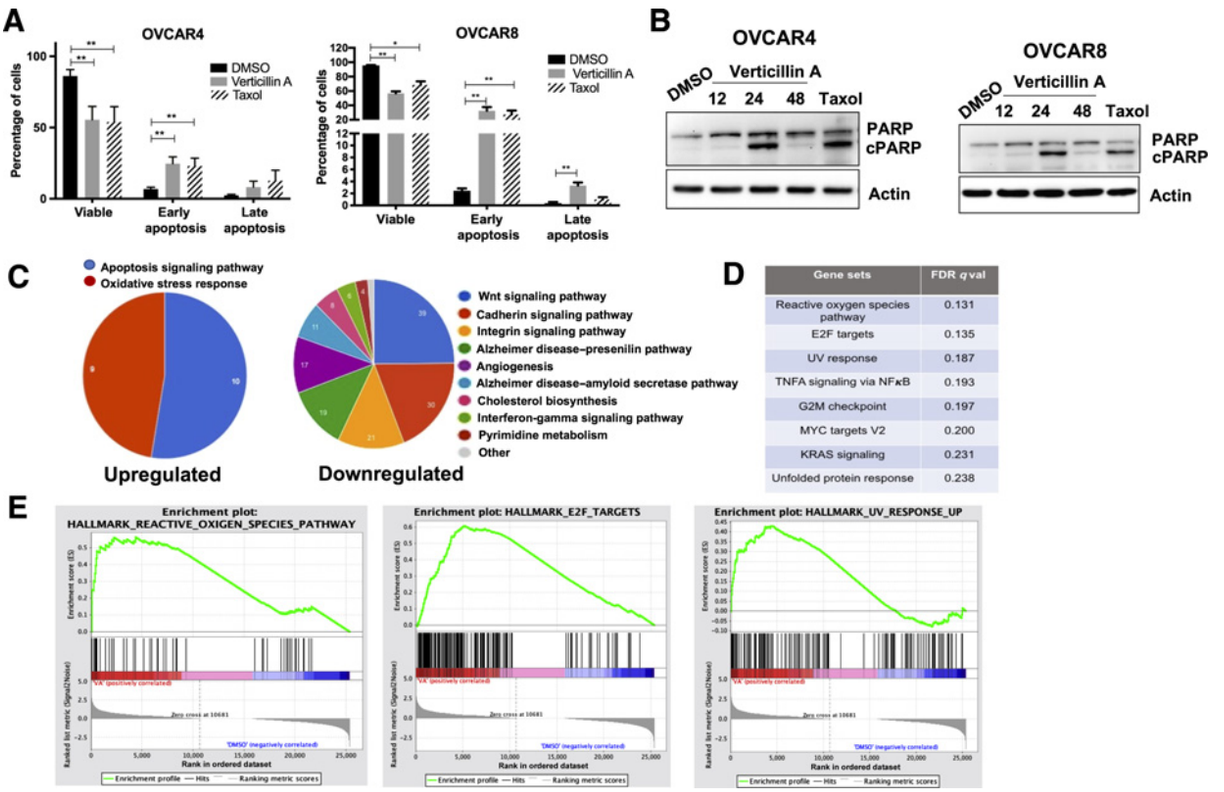

Figure 2.

RNA-sequencing analysis shows upregulation of apoptosis and oxidative stress in verticillin A–treated OVCAR8 cells. **A,** OVCAR4 and OVCAR8 cells were treated with vehicle (DMSO), verticillin A (50 nmol/L), and taxol (10 nmol/L) for 24 hours, stained with Annexin V-FITC and propidium iodide, and analyzed by Nexcelom Cellometer. Each experiment was performed in three biological replicates, and data represent mean ± SEM. Statistics were generated with one-way ANOVA with Dunnett multiple comparisons with vehicle control within each group. **B,** Immunoblot analysis of whole-cell lysates of OVCAR4 and OVCAR8 cells probed for apoptotic marker (cPARP), and actin was used as a loading control. **C,** OVCAR8 cells were treated with vehicle and verticillin A for 24 hours. Chart denotes pathway analysis of the upregulated genes by PANTHER analysis. **D,** Table represents pathways identified by GSEA for OVCAR8 cells treated with vehicle control and verticillin A. **E,** Gene set enrichment plots based upon GSEA of transcripts altered by verticillin A treatment in OVCAR8 cells.

probe becomes fluorescent, which was analyzed via fluorescence microscopy. H_2O_2 is known to induce DNA damage via ROS generation and was used as a positive control. As shown in **Fig. 3A**, treatment with verticillin A and H_2O_2 led to ROS formation.

Oxidative stress–mediated apoptosis is frequently caused by damage to DNA (24). To determine whether verticillin A treatment caused DNA damage in HGSOC cells, OVCAR4 and OVCAR8 cells were treated with verticillin A for 24 hours and an alkaline comet assay was performed. As shown in **Fig. 3B**, verticillin A caused DNA damage, which was observed by DNA migration smear (comet tail) under electrophoretic conditions. Cells treated with vehicle control did not form a comet tail, whereas cells treated with H_2O_2 formed a comet tail. Analysis of comet tails showed a 5-fold increase in comet tail moment in verticillin A–treated cells relative to vehicle control.

To confirm this observation, an immunofluorescence staining was performed for nuclear γH2A.X, which is a marker for DNA damage response pathways. As shown in **Fig. 3C**, a significant increase in number of γH2A.X foci was observed for verticillin A–treated cells relative to vehicle control. Consistent with the immunofluorescence analysis, expression as measured by blots of γH2.AX was found to be increased in verticillin A–treated OVCAR4 and OVCAR8 cells in a time-dependent manner (**Fig. 3D**). A pathway leading to oxidative stress might be expected to induce mitochondrial toxicity, which is a common mode of failure for experimental agents in clinical trials. However, using a standard Mitochondrial ToxGlo kit, verticillin A did not demonstrate mitochondrial toxicity (Supplementary Fig. S4).

Verticillin A–mediated apoptosis and DNA damage are reversed by free radical quencher N-acetyl-L-cysteine

To confirm whether blocking oxidative stress would reduce DNA damage and apoptosis, cells were cotreated with verticillin A and antioxidant N-acetyl-L-cysteine (NAC). NAC is a ROS quencher and a combined treatment of verticillin A and NAC completely blocked apoptosis based on PARP cleavage (**Fig. 4A**). Consistent with the Western blot analysis, annexin V/propidium iodide staining showed that NAC blocked verticillin A–stimulated apoptosis in OVCAR4 and OVCAR8 cells (**Fig. 4B**). Similarly, induction of γH2A.X expression and comet tail was attenuated by NAC as seen in **Fig. 4A** and **C**. This suggested that verticillin A–induced DNA damage and apoptosis was mediated by oxidative stress.

eNP-VA demonstrated reduced liver toxicity relative to free drug

To determine whether verticillin A affected tumor burden *in vivo*, OVCAR8-RFP cells were xenografted intraperitoneally into female

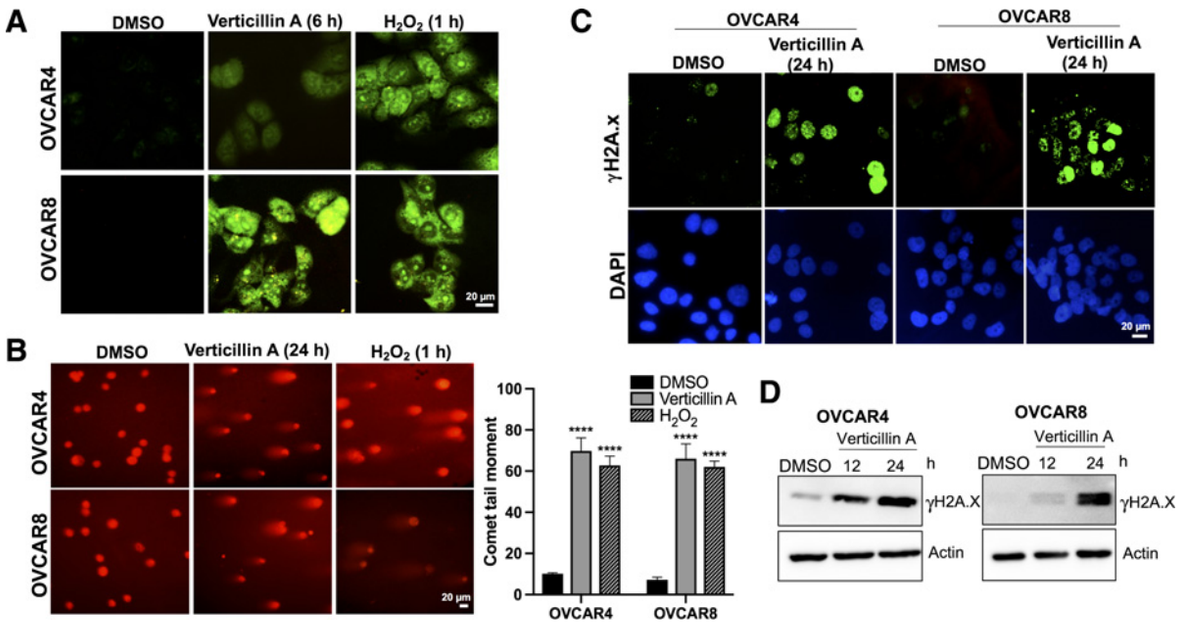

Figure 3.

Verticillin A causes oxidative stress and DNA damage in HGSOC cells. **A,** Verticillin A–induced oxidative stress in OVCAR4 and OVCAR8 cells was measured with CellROX Green reagent in cells treated with vehicle (DMSO), verticillin A (50 nmol/L for 6 hours), and H_2O_2 (50 μmol/L for 1 hour). Images were acquired using 40× objective of a fluorescent microscope. Scale bar, 20 μm. **B,** OVCAR4 and OVCAR8 cells were treated with vehicle, verticillin A (50 nmol/L), and H_2O_2 (50 μmol/L), and alkaline comet assay was performed to analyze DNA damage. Comet tail moment was used to quantify DNA damage by TriTek CometScore software. Each experiment was performed in three biological replicates, and data represent mean ± SEM. Statistics were generated with one-way ANOVA with Dunnett multiple comparisons with vehicle control within each cell line. Scale bar, 20 μm. **C,** Representative images of immunofluorescence staining of γH2A.X foci for OVCAR4 and OVCAR8 cells treated with vehicle and verticillin A (50 nmol/L) for 24 hours. Nuclei were stained by DAPI (0.1 μg/mL). Scale bar, 20 μm. **D,** Immunoblot analysis of whole-cell lysates of OVCAR4 and OVCAR8 cells treated with vehicle and verticillin A (50 nmol/L) for different timepoints. Lysates were probed for DNA damage marker γH2A.X, and actin was used as a loading control.

athymic nude mice. Tumors were allowed to form for 4 weeks and once all the mice displayed detectable tumors, the animals were treated with verticillin A and vehicle control (Cremophor EL/EtOH). However, animals treated with verticillin A showed significant gross morphologic liver damage at the time of sacrifice (**Fig. 5A**). These observations suggested that verticillin A exerted a nonspecific cytotoxic effect *in vivo*. To confirm this, dose–response curves were performed using two noncancerous cell lines. Human ovarian surface epithelial cells IOSE80 and human fallopian tube epithelial secretory cells FT33 were treated with verticillin A and vehicle control (DMSO) for 3 days. As shown in **Fig. 5B**, verticillin A inhibited growth of both cancerous and noncancerous cells indicating a nonspecific cytotoxic effect.

To improve the drug specificity toward tumor cells, verticillin A was encapsulated in expansile nanoparticles (verticillin A-eNPs) that have been shown to, following intraperitoneal administration, localize to intraperitoneal tumors of ovarian, mesothelial, and pancreatic origin (16, 17, 25–27). Unloaded-eNPs were used as a negative control. These eNPs localize to tumors via materials-based targeting and, following internalization via macropinocytosis, release the encapsulated verticillin A upon encountering the acidic late endosome, thus reducing nonspecific toxicity and increasing drug delivery to the tumor (16, 17). To determine whether verticillin A–loaded nanoparticles were still active, verticillin A-eNPs and eNPs were evaluated in an *in vitro* cytotoxicity assay using three HGSOC cell lines (OVSAHO, OVCAR4, and OVCAR8). As shown in **Fig. 5C**, verticillin A-eNPs showed potent cytotoxicity with IC_{50} values of 44 nmol/L, 29 nmol/L, and 32 nmol/L in OVSAHO, OVCAR4, and OVCAR8 cells, respectively. Interestingly, IC_{50} values of verticillin A-eNPs were similar to free compound in all three HGSOC cell lines tested, confirming that encapsulation in nanoparticles did not reduce the activity and potency of verticillin A (**Figs. 1A** and **5C**). Unloaded-eNPs did not exert a cytotoxic effect on any of the cell lines (**Fig. 5C**).

Verticillin A reduces tumor burden *in vivo*

To evaluate the ability of verticillin A-eNPs to reduce *in vivo* tumor burden, OVCAR8-RFP cells were xenografted intraperitoneally in athymic nude mice and tumors were allowed to form for 4 weeks. The mice were treated with unloaded-eNPs and verticillin A-eNPs every other day for 12 days at a dose of 0.5 mg/kg. As shown in **Fig. 6A–C**, animals treated with verticillin A-eNPs had significantly less tumor burden based on average radiant efficiency measured with IVIS and had no measurable change in body weight. Interestingly, eNPs and verticillin A-eNPs did not cause the same gross morphologic liver damage that was seen in mice treated with free verticillin A, suggesting that encapsulation into the eNPs allowed for drug efficacy while reducing liver toxicity. IHC analysis showed an increased staining for γH2A.X and cPARP for tumors from verticillin A-eNP–treated animals (**Fig. 6E**). This indicates that verticillin A reduced tumor burden by causing DNA damage and apoptosis, which was consistent with the *in vitro* findings.

Discussion

New therapies are needed to treat HGSOC- and metastasis-related lethality from the disease. Nearly 60% of all FDA-approved anticancer

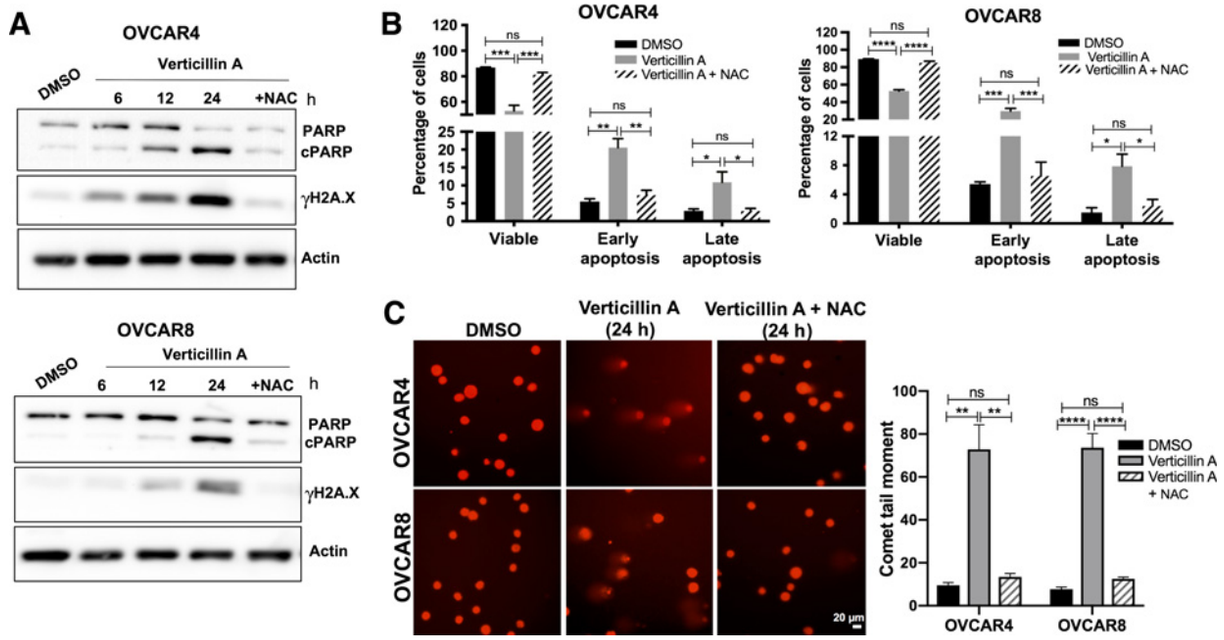

Figure 4.

Verticillin A–mediated apoptosis and DNA damage are reversed by free radical quencher NAC. **A,** Immunoblot analysis of whole-cell lysates of OVCAR4 and OVCAR8 cells treated with vehicle (DMSO), verticillin A (50 nmol/L), and combination of verticillin A (50 nmol/L) and NAC (1 mmol/L) for 24 hours. Lysates were probed for apoptosis and DNA damage markers. Actin was used as a loading control. **B,** OVCAR4 and OVCAR8 cells were treated with vehicle, verticillin A (50 nmol/L), and combination of verticillin A (50 nmol/L) and NAC (1 mmol/L) for 24 hours, stained with Annexin V-FITC (AV) and propidium iodide (PI), and analyzed by Nexcelom Cellometer. Each experiment was performed in three biological replicates, and data represent mean ± SEM. Statistics were generated with one-way ANOVA with Tukey multiple comparisons within each group. **C,** OVCAR4 and OVCAR8 cells were treated with vehicle, verticillin A (50 nmol/L), and combination of verticillin A (50 nmol/L) and NAC (1 mmol/L) for 24 hours. Alkaline comet assay was performed to analyze DNA damage. Comet tail moment was used to quantify DNA damage by TriTek CometScore software. Each experiment was performed in three biological replicates, and data represent mean ± SEM. Statistics were generated with one-way ANOVA with Tukey multiple comparisons within each cell line. Scale bar, 20 μm; ns, not significant.

drugs are derived from nature, and it remains a promising source for new drug leads, particularly due to the chemical diversity (28, 29). This study found that verticillin A, a fungal metabolite, caused cytotoxicity in HGSOC cells and when encapsulated into a nanoparticle, it reduced tumor burden *in vivo*. Mechanistically, treatment with verticillin A caused DNA damage and induced apoptotic cell death in HGSOC cells. A complete reversal of DNA damage and apoptosis occurred by combining verticillin A with the antioxidant, NAC. This indicated that verticillin A–mediated cytotoxicity occurred in part due to induction of DNA damage from oxidative stress. RNA-sequencing analysis of verticillin A–treated OVCAR8 cells supported this finding as oxidative stress and apoptosis pathways were significantly upregulated relative to vehicle-treated cells. Encapsulation of verticillin A in eNPs improved drug specificity, reduced toxicity and, more importantly, caused a significant reduction of tumor burden *in vivo*.

Epigenetic alterations such as histone modifications are reversible and regulate gene expression by transcriptional activation and/or repression (30, 31). A number of studies have shown that alterations in histone methylation and acetylation levels play a role in ovarian cancer metastasis, resensitization toward cisplatin, and overall patient survival (30, 32–35). Mechanistically, verticillin A targets HMTases, causing apoptotic cell death and improved chemotherapeutic response in colon and pancreatic tumor cell models (12, 13, 23). Consistent with previous studies in colon and pancreatic cancer, verticillin A altered histone modifications in OVCAR8, a HGSOC cell line. Global histone modification mapping using mass spectrometry revealed several histone modifications after treatment of OVCAR8 cells with verticillin A, including a reduction in H3K9me2, which was reported in colon cancer, along with changes in H3K14 acetylation marks (12). Interestingly, a reduction in H3K36me2 was found after verticillin A treatment. H3K36me2 is reported to play a role in double-strand break repair, specifically by stabilizing DNA repair factors (36). In addition to our findings that verticillin A induced DNA damage, reduction in H3K36me2 also suggests that verticillin A may impact DNA double-strand break repair.

Verticillin A showed concentration-dependent cytotoxicity in HGSOC cell lines OVSAHO, OVCAR4, and OVCAR8 by causing apoptosis. Moreover, verticillin A induced oxidative stress in HGSOC cells leading to DNA damage, as confirmed by comet assay and immunostaining for γH2.AX foci. This was supported by RNA-sequencing analysis, which showed significant upregulation of oxidative stress and apoptosis pathways after verticillin A treatment. Induction of apoptosis by verticillin A is reported in colon and pancreatic cancer, however, its role in oxidative stress was unknown (12, 13, 14). In colon and pancreatic cancer cells, verticillin A treatment reduced H3K9me3 levels, which increased expression of proapoptotic protein Bax (12, 14, 23). This is consistent with our findings in OVCAR4 and OVCAR8 cells suggesting that histone modifications caused by verticillin A lead to apoptotic cell death by increasing Bax expression. Verticillin A is a selective inhibitor of HMTase G9a and expression of G9a correlates with tumor aggressiveness and reduced survival in patients with ovarian

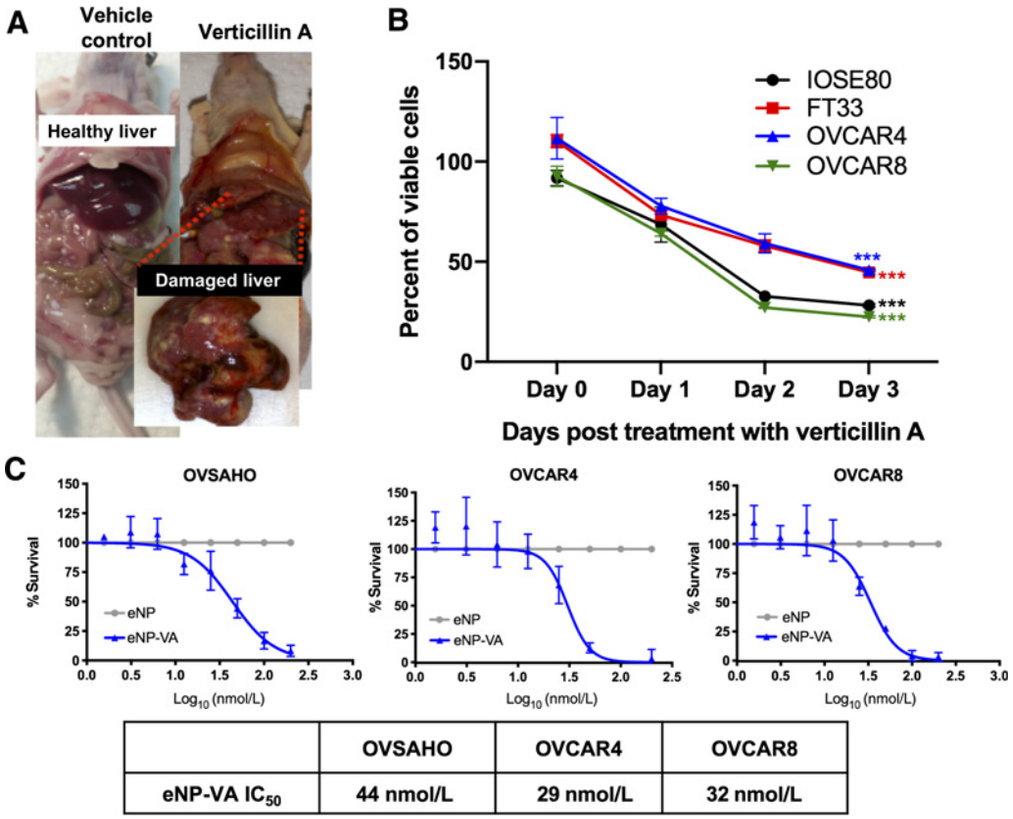

	OVSAHO	OVCAR4	OVCAR8
eNP-VA IC_{50}	44 nmol/L	29 nmol/L	32 nmol/L

Figure 5.

eNP-VA demonstrate reduced liver toxicity relative to free drug. **A,** OVCAR8-RFP cells were xenografted intraperitoneally to form tumors. Mice were dosed with verticillin A and vehicle (Cremophor EL/EtOH) once in 7 days (dosage: 0.5 mg/kg). Representative images show liver damage in verticillin A–treated animals. **B,** Four ovarian cell lines (IOSE80, FT33, OVCAR4, and OVCAR8) were treated with vehicle (DMSO) and verticillin A (50 nmol/L) for 72 hours. Dose–response curves were generated and normalized to vehicle control. Each experiment was performed in three biological replicates, and data represent mean ± SEM. Statistics were generated with Student *t* test for day 0 and day 3 within each cell line. **C,** OVSAHO, OVCAR4, and OVCAR8 cells were treated with eNP-VA and empty nanoparticles (eNP) for 72 hours. Dose–response curves were generated and normalized to eNP. Data represent mean ± SEM from three biological replicates. IC_{50} values are denoted in the table.

cancer (12, 37). Studies using small molecules targeting G9a indicated that blocking G9a caused oxidative stress in breast cancer cells (38). In another study using colorectal cancer cells, downregulation of G9a caused DNA damage and inhibited cell proliferation (39). Verticillin A reduced H3K9me2 levels as demonstrated by histone profiling of OVCAR8 cells and G9a is a repressive HMTase for H3K9me2 (12). Taken together, these finding suggest that verticillin A treatment induced oxidative stress and apoptosis possibly by G9a inhibition in HGSOC.

A challenge with chemotherapeutic agents, particularly hydrophobic ones derived from nature, is to identify a delivery method that enables drug to accumulate therapeutic concentrations within the target tissue while minimizing, or averting altogether, adverse systemic toxicities. For example, taxol, which was first reported in 1971, was not considered a promising drug in terms of solubility, toxicity, and large-scale production (40–42). However, tremendous progress has been made in the past four decades making taxol one of the most effective chemotherapeutic drugs, particularly in first-line therapy for ovarian cancer (43–45). Intraperitoneal administration of free verticillin A, solubilized in Cremophor EL/EtOH, as a means to address its low solubility, resulted in liver toxicity. Shorter studies using verticillin A intraperitoneally did not report significant liver toxicity, however, studies performed using peripheral nerve sheath tumor cells report toxicity and weight loss in mice treated with verticillin A (12, 22). The specific mechanism(s) of verticillin A–induced hepatotoxicity is unknown and further toxicology studies are required. To overcome the toxic effects induced by verticillin A, and to enhance solubility, a well-characterized nanoparticle-based drug delivery system, the eNP was used (16, 17, 46). Previously, eNPs have been used to deliver other cytotoxic natural products (e.g., taxol) with high specificity to peritoneal tumors (16, 17, 25–27, 47). As a result of their unique materials-based targeting mechanism, eNPs afford 10- to 100-fold higher intratumoral drug concentrations than are achieved with free drug and show remarkable efficacy (e.g., doubling of survival compared with free drug controls; ref. 16). In terms of ovarian cancer, paclitaxel encapsulated eNPs demonstrated better uptake by tumor cells, as well as reduced tumor reoccurrence *in vivo* compared with paclitaxel alone (27). In this study, eNPs delivered verticillin A to ovarian tumors and consistent with previous studies, the eNP formulation demonstrated improved drug efficacy with reduced hepatotoxicity. Verticillin A-eNP–treated animals showed significant reduction in tumor burden in comparison with the eNP-treated animals. Furthermore, histologic studies confirmed induction of DNA damage and apoptosis in verticillin A-eNP–treated animals consistent with our *in vitro* findings.

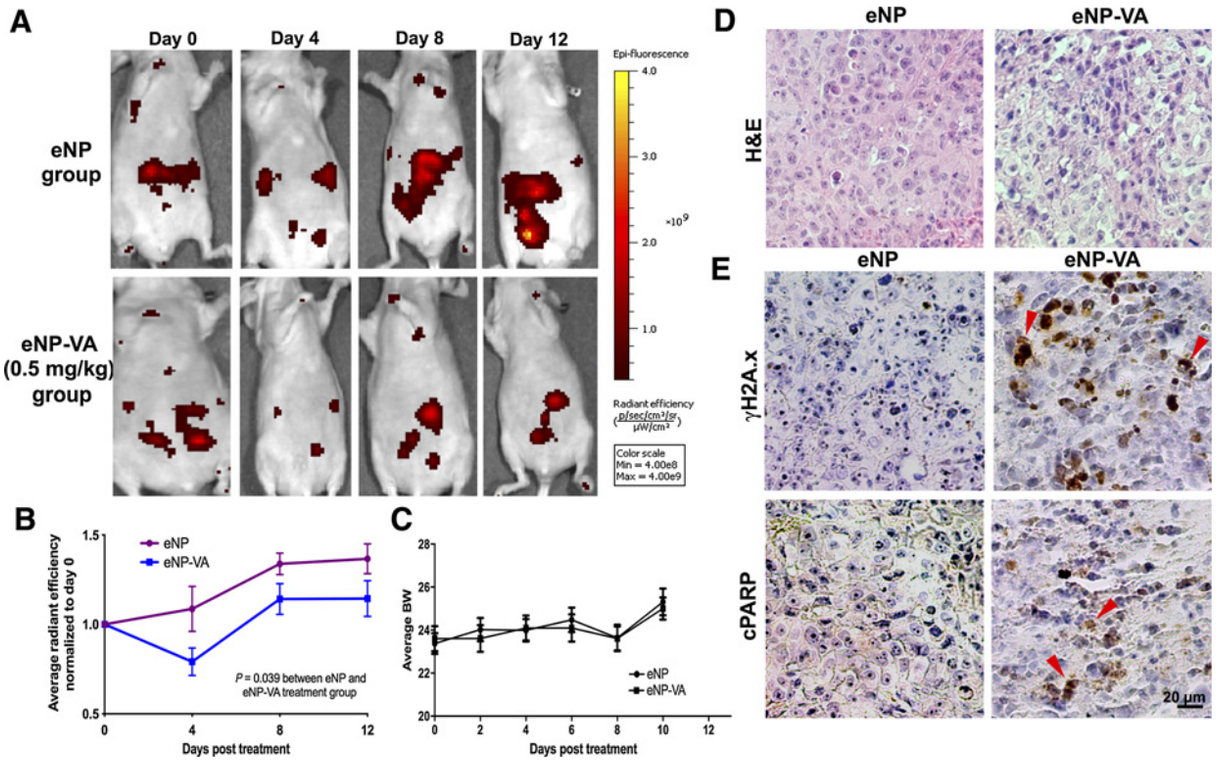

Figure 6.

Verticillin A reduces tumor burden *in vivo.* **A,** OVCAR8-RFP cells were xenografted intraperitoneally to form tumors. Mice were dosed with eNP-VA and eNP once every 2 days for total 12 days (dosage: 0.5 mg/kg). Representative images show IVIS images of tumors in mice on days 0, 4, 8, and 12 of drug treatment. **B,** Quantification of tumor burden (average radiant efficiency as measured with IVIS imaging) normalized to day 0. Statistics were performed using two-way ANOVA relative to vehicle control. **C,** Quantification of average body weight (BW) of the mice during the course of treatment with eNP and eNP-VA. **D,** H & E staining showing the histomorphology of paraffin-embedded tumor tissue sections of eNP and eNP-VA–treated animals. **E,** IHC of γH2A.X and cPARP staining as markers of DNA damage and apoptosis is shown from tumors of animals treated with eNP and eNP-VA. Scale bar, 20 μm.

Another challenge with natural products, particularly with verticillin A, despite its enormous promise as an anticancer agent, is the inability to produce verticillin A in large quantities. However, sufficient quantities of verticillin A for preclinical studies are now possible by cultivation of a unique fungal strain and optimization of its fermentation conditions, such that 50–150 mg of verticillin A can be generated monthly on the laboratory scale (11). An adequate supply of verticillin A now exists for preclinical studies, which is being used to fully explore the pharmacologic potential of this drug lead.

In conclusion, our findings validate verticillin A as a potent cytotoxic agent in HGSOC cells by inducing DNA damage. Encapsulation of verticillin A in an eNP improves drug efficacy, reduces toxicity, and highlights the advantages of marrying natural products/anticancer research with nanoparticle drug delivery systems to address a clinical challenge. Continued investigation of verticillin A, verticillin analogues, and the eNP delivery system will provide key data for preparing an optimized efficacious formulation worthy of large animal pharmacokinetic studies and bring us one step closer to a promising therapy for patients with ovarian cancer.

Disclosure of Potential Conflicts of Interest

A.H. Colby is a co-founder and director of research (paid consultant) at, and has ownership interest (including patents) in, Ionic Pharmaceuticals, LLC. No potential conflicts of interest were disclosed by the other authors.

Authors' Contributions

Conception and design: A. Salvi, M.W. Grinstaff, N.H. Oberlies, J.E. Burdette

Development of methodology: A. Salvi, C.S.M. Amrine, A. Russo, Z. Mattes, C.J. Pearce, N.H. Oberlies, J.E. Burdette

Acquisition of data (provided animals, acquired and managed patients, provided facilities, etc.): A. Salvi, C.S.M. Amrine, J.R. Austin, K. Kilpatrick, D. Lantvit, E. Calderon-Gierszal, Z. Mattes

Analysis and interpretation of data (e.g., statistical analysis, biostatistics, computational analysis): A. Salvi, C.S.M. Amrine, J.R. Austin, K. Kilpatrick, A. Russo, E. Calderon-Gierszal, Z. Mattes, J.E. Burdette

Writing, review, and/or revision of the manuscript: A. Salvi, C.S.M. Amrine, A. Russo, E. Calderon-Gierszal, C.J. Pearce, M.W. Grinstaff, A.H. Colby, N.H. Oberlies, J.E. Burdette

Administrative, technical, or material support (i.e., reporting or organizing data, constructing databases): A. Salvi, C.J. Pearce

Study supervision: J.E. Burdette

Other (isolation and purification of verticillin A used in this study, as well as synthesizing the nanoparticles, analyzing, characterizing, and calculating their encapsulation efficiency and also participated in writing the article): C.S.M. Amrine

Acknowledgments

This work was supported in part by grants P01CA125066 awarded to Dr. Alan Kinghorn and R01CA227433 to J.E. Burdette from the NCI of the NIH. Grant #T32AT007533 was awarded to Dr. Guido Pauli for which J.R. Austin is a recipient by the Office of the Director, NIH and the National Center for Complementary & Integrative Health. IVIS imaging was performed using Xenogen IVIS Spectrum Imager at University of Illinois, Chicago Research Resource Center's Center for

Cardiovascular Research and Physiology Core. Proteomics services were performed by the Northwestern Proteomics Core Facility, generously supported by NCI CCSG P30 CA060553 awarded to Dr. Neil L. Kelleher at the Robert H Lurie Comprehensive Cancer Center and the National Resource for Translational and Developmental Proteomics supported by P41 GM108569 awarded to Dr. Neil L. Kelleher. RNA-sequencing analysis was performed at the NUSeq Core Facility, which is supported by the Northwestern University Center for Genetic Medicine, Feinberg School of Medicine, and Shared and Core Facilities of the University's Office for Research.

The costs of publication of this article were defrayed in part by the payment of page charges. This article must therefore be hereby marked *advertisement* in accordance with 18 U.S.C. Section 1734 solely to indicate this fact.

Received February 28, 2019; revised June 6, 2019; accepted September 9, 2019; published first January 3, 2020.

References

1. Siegel RL, Miller KD, Jemal A. Cancer statistics, 2017. CA Cancer J Clin 2017;67:7–30.
2. American Cancer Society. Cancer facts and figures 2019. Atlanta, GA:American Cancer Society; 2019. Available from: https://www.cancer.org/research/cancer-facts-statistics/all-cancer-facts-figures/cancer-facts-figures-2019.html.
3. Bowtell DD, Böhm S, Ahmed AA, Aspuria P-J, Bast RC, Beral V, et al. Rethinking ovarian cancer II: reducing mortality from high-grade serous ovarian cancer. Nat Rev Cancer 2015;15:668–79.
4. Korkmaz T, Seber S, Basaran G. Review of the current role of targeted therapies as maintenance therapies in first and second line treatment of epithelial ovarian cancer; in the light of completed trials. Crit Rev Oncol Hematol 2016;98:180–8.
5. Bitler BG, Watson ZL, Wheeler LJ, Behbakht K. PARP inhibitors: clinical utility and possibilities of overcoming resistance. Gynecol Oncol 2017;147:695–704.
6. Herzog TJ, Monk BJ. Bringing new medicines to women with epithelial ovarian cancer: what is the unmet medical need? Gynecol Oncol Res Pract 2017;4:13.
7. Kinghorn AD, DE Blanco EJC, Lucas DM, Rakotondraibe HL, Orjala J, Soejarto DD, et al. Discovery of anticancer agents of diverse natural origin. Anticancer Res 2016;36:5623–37.
8. Figueroa M, Graf TN, Ayers S, Adcock AF, Kroll DJ, Yang J, et al. Cytotoxic epipolythiodioxopiperazine alkaloids from filamentous fungi of the Bionectriaceae. J Antibiot 2012;65:559–64.
9. Katagiri K, Sato K, Hayakawa S, Matsushima T, Minato H. Verticillin A, a new antibiotic from Verticillium sp. J Antibiot 1970;23:420–2.
10. Minato H, Matsumoto M, Katayama T. Studies on the metabolites of Verticillium sp. structures of verticillins A, B, and C. J Chem Soc Perkin 1 1973;17:1819–25.
11. Amrine CSM, Raja HA, Darveaux BA, Pearce CJ, Oberlies NH. Media studies to enhance the production of verticillins facilitated by in situ chemical analysis. J Ind Microbiol Biotechnol 2018;45:1053–65.
12. Paschall AV, Yang D, Lu C, Choi J-H, Li X, Liu F, et al. H3K9 trimethylation silences fas expression to confer colon carcinoma immune escape and 5-fluorouracil chemoresistance. J Immunol 2015;195:1868–82.
13. Lu C, Paschall AV, Shi H, Savage N, Waller JL, Sabbatini ME, et al. The MLL1-H3K4me3 axis-mediated PD-L1 expression and pancreatic cancer immune evasion. J Natl Cancer Inst 2017;109:djw283.
14. Lu C, Yang D, Sabbatini ME, Colby AH, Grinstaff MW, Oberlies NH, et al. Contrasting roles of H3K4me3 and H3K9me3 in regulation of apoptosis and gemcitabine resistance in human pancreatic cancer cells. BMC Cancer 2018;18:149.
15. Zubris KAV, Liu R, Colby A, Schulz MD, Colson YL, Grinstaff MW. In vitro activity of paclitaxel-loaded polymeric expansile nanoparticles in breast cancer cells. Biomacromolecules 2013;14:2074–82.
16. Colby AH, Oberlies NH, Pearce CJ, Herrera VLM, Colson YL, Grinstaff MW. Nanoparticle drug-delivery systems for peritoneal cancers: a case study of the design, characterization and development of the expansile nanoparticle. Wiley Interdiscip Rev Nanomed Nanobiotechnol 2017;9:e1451.
17. Liu R, Colby AH, Gilmore D, Schulz M, Zeng J, Padera RF, et al. Nanoparticle tumor localization, disruption of autophagosomal trafficking, and prolonged drug delivery improve survival in peritoneal mesothelioma. Biomaterials 2016;102:175–86.
18. Vichai V, Kirtikara K. Sulforhodamine B colorimetric assay for cytotoxicity screening. Nat Protoc 2006;1:1112–6.
19. Garcia BA, Mollah S, Ueberheide BM, Busby SA, Muratore TL, Shabanowitz J, et al. Chemical derivatization of histones for facilitated analysis by mass spectrometry. Nat Protoc 2007;2:933–8.
20. Lewellen KA, Metzinger MN, Liu Y, Stack MS. Quantitation of intra-peritoneal ovarian cancer metastasis. J Vis Exp 2016. doi: 10.3791/53316.
21. King SM, Hilliard TS, Wu LY, Jaffe RC, Fazleabas AT, Burdette JE. The impact of ovulation on fallopian tube epithelial cells: evaluating three hypotheses connecting ovulation and serous ovarian cancer. Endocr Relat Cancer 2011;18:627–42.
22. Zewdu A, Lopez G, Braggio D, Kenny C, Constantino D, Bid HK, et al. Verticillin A inhibits leiomyosarcoma and malignant peripheral nerve sheath tumor growth via induction of apoptosis. Clin Exp Pharmacol 2016;6. doi: 10.4172/2161-1459.1000221.
23. Liu F, Liu Q, Yang D, Bollag WB, Robertson K, Wu P, et al. Verticillin A overcomes apoptosis resistance in human colon carcinoma through DNA methylation-dependent upregulation of BNIP3. Cancer Res 2011;71:6807–16.
24. Wiseman H, Halliwell B. Damage to DNA by reactive oxygen and nitrogen species: role in inflammatory disease and progression to cancer. Biochem J 1996;313:17–29.
25. Colby AH, Berry SM, Moran AM, Pasion KA, Liu R, Colson YL, et al. Highly specific and sensitive fluorescent nanoprobes for image-guided resection of sub-millimeter peritoneal tumors. ACS Nano 2017;11:1466–77.
26. Herrera VL, Colby AH, Tan GA, Moran AM, O'Brien MJ, Colson YL, et al. Evaluation of expansile nanoparticle tumor localization and efficacy in a cancer stem cell-derived model of pancreatic peritoneal carcinomatosis. Nanomedicine 2016;11:1001–15.
27. Gilmore D, Schulz M, Liu R, Zubris KAV, Padera RF, Catalano PJ, et al. Cytoreductive surgery and intraoperative administration of paclitaxel-loaded expansile nanoparticles delay tumor recurrence in ovarian carcinoma. Ann Surg Oncol 2013;20:1684–93.
28. Newman DJ, Cragg GM. Natural products as sources of new drugs from 1981 to 2014. J Nat Prod 2016;79:629–61.
29. El-Elimat T, Zhang X, Jarjoura D, Moy FJ, Orjala J, Kinghorn AD, et al. Chemical diversity of metabolites from fungi, cyanobacteria, and plants relative to FDA-approved anticancer agents. ACS Med Chem Lett 2012;3:645–9.
30. Marsh DJ, Shah JS, Cole AJ. Histones and their modifications in ovarian cancer - drivers of disease and therapeutic targets. Front Oncol 2014;4:144.
31. Dawson MA, Kouzarides T, Huntly BJP. Targeting epigenetic readers in cancer. N Engl J Med 2012;367:647–57.
32. Abbosh PH, Montgomery JS, Starkey JA, Novotny M, Zuhowski EG, Egorin MJ, et al. Dominant-negative histone H3 lysine 27 mutant derepresses silenced tumor suppressor genes and reverses the drug-resistant phenotype in cancer cells. Cancer Res 2006;66:5582–91.
33. Wang RH, Zheng Y, Kim HS, Xu X, Cao L, Luhasen T, et al. Interplay among BRCA1, SIRT1, and survivin during BRCA1-associated tumorigenesis. Mol Cell 2008;32:11–20.
34. Hayashi A, Horiuchi A, Kikuchi N, Hayashi T, Fuseya C, Suzuki A, et al. Type-specific roles of histone deacetylase (HDAC) overexpression in ovarian carcinoma: HDAC1 enhances cell proliferation and HDAC3 stimulates cell migration with downregulation of E-cadherin. Int J Cancer 2010;127:1332–46.
35. Balch C, Fang F, Matei DE, Huang TH-M, Nephew KP. Minireview: epigenetic changes in ovarian cancer. Endocrinology 2009;150:4003–11.
36. Fnu S, Williamson EA, De Haro LP, Brenneman M, Wray J, Shaheen M, et al. Methylation of histone H3 lysine 36 enhances DNA repair by nonhomologous end-joining. Proc Natl Acad Sci USA 2011;108:540–5.
37. Hua KT, Wang MY, Chen MW, Wei LH, Chen CK, Ko CH, et al. The H3K9 methyltransferase G9a is a marker of aggressive ovarian cancer that promotes peritoneal metastasis. Mol Cancer 2014;13:189.
38. Kim Y, Kim YS, Kim DE, Lee JS, Song JH, Kim HG, et al. BIX-01294 induces autophagy-associated cell death via EHMT2/G9a dysfunction and intracellular reactive oxygen species production. Autophagy 2013;9:2126–39.
39. Zhang J, He P, Xi Y, Geng M, Chen Y, Ding J. Down-regulation of G9a triggers DNA damage response and inhibits colorectal cancer cells proliferation. Oncotarget 2015;6:2917–27.

40. Wani MC, Taylor HL, Wall ME, Coggon P, McPhail AT. Plant antitumor agents. VI. Isolation and structure of taxol, a novel antileukemic and antitumor agent from Taxus brevifolia. J Am Chem Soc 1971;93:2325–7.
41. Weaver BA. How taxol/paclitaxel kills cancer cells. Mol Biol Cell 2014;25:2677–81.
42. Oberlies NH, Kroll DJ. Camptothecin and taxol: historic achievements in natural products research. J Nat Prod 2004;67:129–35.
43. Crown J, O'Leary M. The taxanes: an update. Lancet 2000;355:1176–8.
44. Oberlies NH, Kroll DJ. Camptothecin and taxol: historic achievements in natural products research. J Nat Prod 2004;67:129–35.
45. Tuma RS. Taxol's journey from discovery to use: lessons & updates. Oncology Times 2003;25:52.
46. Griset AP, Walpole J, Liu R, Gaffey A, Colson YL, Grinstaff MW. Expansile nanoparticles: synthesis, characterization, and in vivo efficacy of an acid-responsive polymeric drug delivery system. J Am Chem Soc 2009; 131:2469–71.
47. Colson YL, Liu R, Southard EB, Schulz MD, Wade JE, Griset AP, et al. The performance of expansile nanoparticles in a murine model of peritoneal carcinomatosis. Biomaterials 2011;32:832–40.

Molecular Cancer Therapeutics

Verticillin A Causes Apoptosis and Reduces Tumor Burden in High-Grade Serous Ovarian Cancer by Inducing DNA Damage

Amrita Salvi, Chiraz Soumia M. Amrine, Julia R. Austin, et al.

Mol Cancer Ther 2020;19:89-100.